CERIA-BASED NANOCATALYSTS FOR CO OXIDATION AND SOOT COMBUSTION

T. Andana, M. Piumetti, S. Bensaid*, D. Fino, N. Russo and R. Pirone
*samir.bensaid@polito.it
Department of Applied Science and Technology, Politecnico di Torino,
Corso Duca degli Abruzzi 24, 10129 Torino, Italy

Abstract
We synthesized novel ceria nanocubes doped with zirconium and praseodymium via the hydrothermal procedure (namely pure CeO_2, $CeZrO_2$, $CePrO_2$, and $CePrZrO_2$) For comparison, a set of similar ceria catalysts was prepared by the solution combustion synthesis (SCS). The catalysts were tested for the CO and soot oxidation. These materials showed different surface reducibility, as measured by H_2-TPR, CO-TPR and Soot-TPR, despite their comparable compositions (Zr = Pr = 10 at.%). Soot-TPR appears a suitable characterization technique for soot oxidation catalysts, whereas CO-TPR technique allows to better discriminate among the CO oxidation activities. Praseodymium contributes positively towards the soot oxidation activity. On the other hand, it has an adverse effect on the CO oxidation over the same catalysts, as compared to pure ceria. The incorporation of zirconium into the ceria lattice does not have a direct beneficial effect on the soot oxidation activity, although it increases the catalyst performances for the CO oxidation.

Introduction
Many studies have shown that modifying the textural and structural properties of ceria-based catalysts, it is possible to improve their oxidation activity towards CO oxidation and soot combustion [1-5]. In particular, CeO_2-nanocubes prepared through the hydrothermal synthesis appear the most effective ceria catalysts for both the oxidation reactions, since they exhibit a rich population of highly reactive (110) and (100)-type planes, at variance of the "classical" ceria prepared by the solution combustion synthesis (SCS) [6]. On the other hand, we investigated sets of $CeZrO_2$ and Ce-PrO_2 nanocatalysts, in which either Zr or Pr species were embedded into the lattice to promote the formation of crystallographic defects [7-10]. The latter are highly desirable in metal oxide catalysts since they can enhance the number of oxygen vacancies (O_v) and hence the electronic properties are favored, namely the mobility of electrons and negatively charged ions in the solid framework.
We addressed this work to study the geometric and electronic effects of ceria-based catalysts (ternary oxides, binary oxides and pure CeO_2, prepared via the hydrothermal and SCS methods) towards the oxidation activity.
CO and soot catalyzed oxidations are "structure-sensitive reactions" and appear sufficiently representative for explaining the shape-control and element-doping

effects on the catalytic activity. The physico-chemical properties of the prepared materials were investigated using complementary techniques.

Experimental

Materials preparation

The synthesis procedures have been described in our previous studies [7-10]. During a typical hydrothermal synthesis, the $CeZrPrO_2$ sample (denoted as "$Ce_{0.8}Zr_{0.1}Pr_{0.1}O_2$-NP", where NP stands for nanoparticles and the subscripts 0.8, 0.1 or 0.1 indicates the at.% of Ce, Zr and Pr, respectively) is derived from a mixture of $Ce(NO_3)_3$, $ZrO(NO_3)_3$ and $Pr(NO_3)_3$. The nitrate salt solution was transferred into the basic solution and then transferred into a 200-ml autoclave heated at 180 °C for 24 h. The clean precipitate was calcined at 550 °C for 4 h. For comparison, the ternary counterpart (denoted as "$Ce_{0.8}Zr_{0.1}Pr_{0.1}O_2$-SCS") was prepared by the solution combustion synthesis. Analogous approaches were used to prepare the $CeZrO_2$ catalysts (denoted as "$Ce_{0.9}Zr_{0.1}O_2$-NP" and "$Ce_{0.9}Zr_{0.1}O_2$-SCS") and $CePrO_2$ ($Ce_{0.9}Pr_{0.1}O_2$-NP and $Ce_{0.9}Pr_{0.1}O_2$-SCS). Finally, two pure ceria samples were prepared (CeO_2-NP and CeO_2-SCS) according to the procedure reported elsewhere [7].

Catalysts characterization

Powder X-ray diffraction (XRD) analysis was carried out in an X'Pert Philips PW3040 diffractometer using Cu Kα radiation. The peaks were identified using the Powder Diffraction File PDF-2 database from International Centre of Diffraction Data (ICDD). BET surface areas and pore volumes of the samples were obtained by the N_2 sorption at -196 °C performed in a Micrometrics ASAP 2020 instrument. Sample pretreatment prior to analysis was done by heating the powder at 200 °C for 2 h. Morphological features of the catalysts were investigated through field emission-scanning electron microscope (FESEM Zeiss Merlin, Gemini-II column). The element-content was determined through EDS analysis. Different spots were selected in representative zones of the sample. Reducibility of the catalysts was assessed by CO-TPR performed in a temperature-programmed oxidation (TPO) setup equipped with continuous gas analyzers, a fixed bed reactor with an inner diameter of 4 mm and an electric PID-regulated furnace.

Catalytic activity

Catalytic activity of the samples was tested in a temperature-programmed oxidation (TPO) setup, comprising a quartz U-tube micro-reactor, a PID-regulated furnace, a K-type thermocouple placed at the reactor inlet in such a way that its tip is as close as possible to reactor bed and a non-dispersive infrared (NDIR) analyzer. *CO oxidation tests:* the bed reactor contains 100 mg of catalyst. A gaseous mixture of 1000 ppm-vol CO and 10%-vol O_2 in N_2 is fed to the reactor while the furnace heats up gradually from ambient temperature (heating ramp at 5 °C min^{-1}) to a certain temperature at which CO is fully converted to CO_2. *Soot combustion tests:*

the bed reactor consists in a mixture of 150 mg of SiO_2, 45 mg of catalyst and 5 mg of soot ball-milled for 15 minutes to get a "tight" soot-catalyst contact. Then, 100 ml min^{-1} oxidizing gas (10%-vol O_2 in N_2) is fed to the reactor while the furnace heats up gradually from ambient temperature to 700 °C (heating rate of 5 °C min^{-1}).

Results and discussion

As a whole, the cubic fluorite structure of CeO_2 (ICDD Reference no. 01-081-0792) marked by the (111), (200), (220), (311) and (222) planes, is retained for pure cerias, binary and ternary compounds.

Table 1. BET surface areas and total pore volumes of the prepared samples

Sample	SSA (m^2 g^{-1})	V_T (cm^3 g^{-1})
$Ce_{0.8}Zr_{0.1}Pr_{0.1}O_2$-NP	7	0.01
$Ce_{0.8}Zr_{0.1}Pr_{0.1}O_2$-SCS	38	0.06
$Ce_{0.9}Zr_{0.1}O_2$-NP	2	0.01
$Ce_{0.9}Zr_{0.1}O_2$-SCS	20	0.03
$Ce_{0.9}Pr_{0.1}O_2$-NP	9	0.03
$Ce_{0.9}Pr_{0.1}O_2$-SCS	33	0.04
CeO_2-NP	6	0.02
CeO_2-SCS	43	0.04

Table 1 shows the BET surface areas (SSA) and total pore volumes (V_T) of the prepared catalysts derived from the N_2 physisorption at -196 °C. As a whole, the specific surface areas of the nanostructured systems are significantly lower (2-9 m^2 g^{-1}) than those of the SCS-based samples (33-43 m^2 g^{-1}). Moreover, it can be observed that the presence of Zr, Pr dopants slightly improves the textural properties of the CeO_2-nanostructures, but not those of the SCS-based materials. The lowest BET surface area and pore volume (SSA = 4 m^2g^{-1} and V_T = 0.01 cm^3g^{-1}) appear for the Ce-NC and Ce-NR catalyst

FESEM images on Figure 1 were obtained to confirm the morphology of the samples. It is evident that hydrothermal synthesis leads to well-defined nanostructures, as seen on images in the first row. The CeO_2-NP exhibits perfect cubic shapes whose size varies between 300 and 400 nm. Smaller nanocubic shapes (200-300 nm) are still maintained in the $Ce_{0.9}Pr_{0.1}O_2$-NP sample despite the incorporation of Pr, most likely due to the similarity of Ce and Pr oxides' crystal structures. The addition of Zr in the $Ce_{0.9}Zr_{0.1}O_2$-NP sample, on the contrary, changes the shape into nanopolyhedra with smaller size (ca. 20-30 nm). The $Ce_{0.8}Zr_{0.1}Pr_{0.1}O_2$-NP sample, the trimetallic oxide, is surprisingly constituted of distorted nanocubes (100-300 nm); praseodymium promotes the particle reduction while zirconium contributes to the particle distortion The SCS-based samples (all images on the second row), on the other hand, exhibit a sponge-like structure

constituted of polycrystalline agglomerates thanks to the excessive amount of gas released during the synthesis

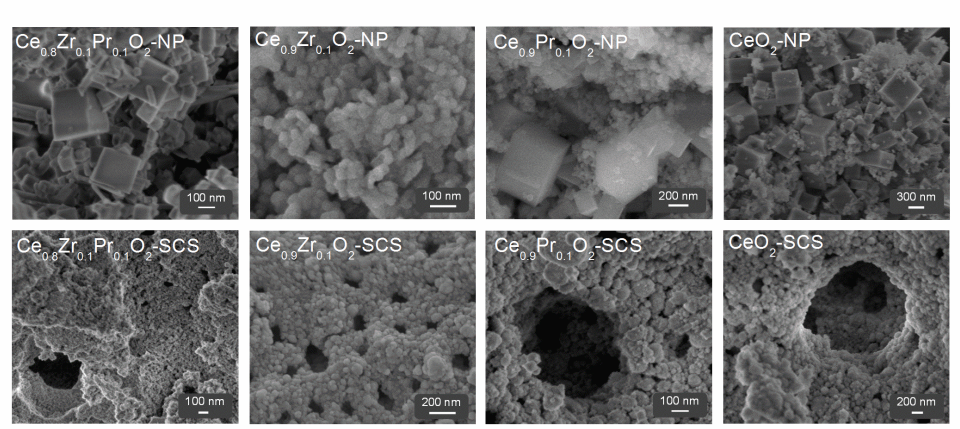

Figure 1. FESEM images of the prepared samples

Reducibility of the catalysts was investigated in a series of CO-TPR analyses, whose results for nanostructured and SCS-based catalysts shown on Figure 2A and B, respectively. The low-temperature reduction peaks, reflecting the surface oxygen consumption, appear in the 300-500 °C range and show the following increasing reducibility order for the nanostructures:

$Ce_{0.8}Zr_{0.1}Pr_{0.1}O_2\text{-}NP \approx Ce_{0.9}Pr_{0.1}O_2\text{-}NP < CeO_2\text{-}NP \approx Ce_{0.9}Zr_{0.1}O_2\text{-}NP$

On the other hand, the reducibility for the SCS-based catalysts follows this order:

$$Ce_{0.9}Zr_{0.1}O_2\text{-}SCS < CeO_2\text{-}SCS < Ce_{0.9}Pr_{0.1}O_2\text{-}SCS < Ce_{0.8}Zr_{0.1}Pr_{0.1}O_2\text{-}SCS$$

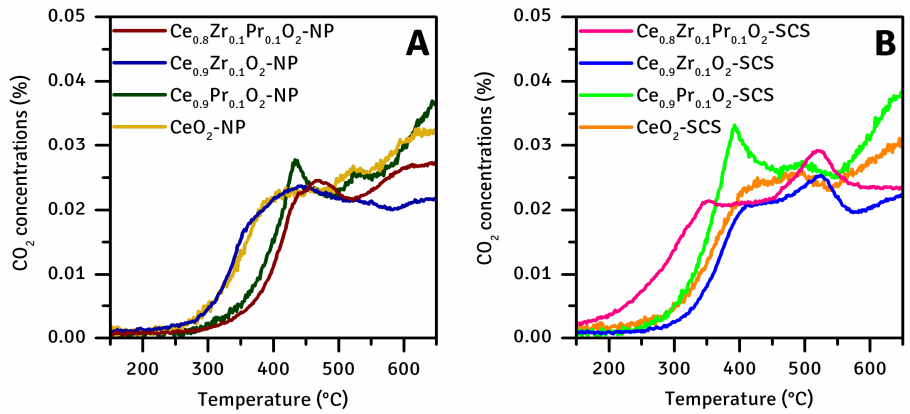

Figure 2. CO-TPR results of the prepared samples

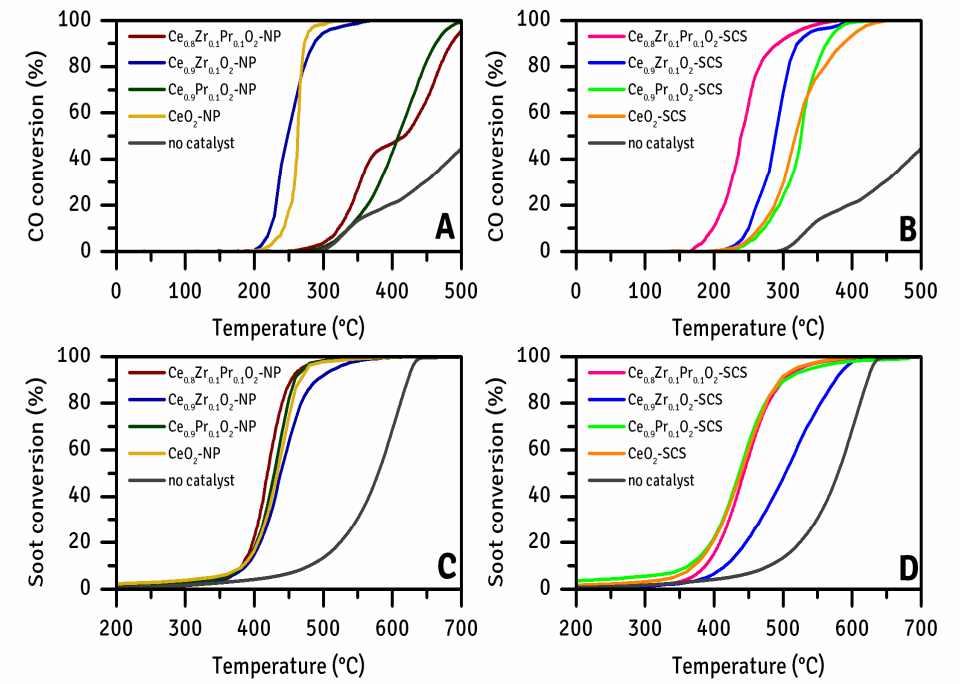

Figure 3. Soot and CO conversions as functions of temperature over the prepared samples

The two sets of samples have opposite trends in terms of surface reducibility with CO, although they have comparable chemical compositions. The insertion of Pr species into the ceria framework gives better reducibility for the SCS-based catalysts, as the shift of peaks to low temperature range is noticeable. Both the $Ce_{0.9}Zr_{0.1}O_2$-NP and CeO_2 appears to be the most performing catalysts for CO oxidation under anaerobic conditions, despite their very low textural properties. This result confirms the high availability of surface redox centres for the CO oxidation.

Figure 3 finally shows soot and CO conversions as functions of temperature, obtained during the series of catalytic tests. In general, all the catalysts improve greatly the CO conversion (Fig.3A and B), whereas only ca. 30% of CO converts naturally to CO_2 at 450 °C. For the nanostructured materials, the following increasing oxidation activity order can be designed:

$$Ce_{0.9}Pr_{0.1}O_2\text{-}NP \approx Ce_{0.8}Zr_{0.1}Pr_{0.1}O_2\text{-}NP < CeO_2\text{-}NP \approx Ce_{0.9}Zr_{0.1}O_2\text{-}NP$$

whereas for the SCS-based catalysts, the increasing order is:

$$CeO_2 \approx Ce_{0.9}Pr_{0.1}O_2\text{-}SCS < Ce_{0.9}Zr_{0.1}O_2\text{-}SCS < Ce_{0.8}Zr_{0.1}Pr_{0.1}O_2\text{-}SCS$$

The catalytic activity trends are in fair agreement with the CO-TPR data (*vide supra*), thus confirming that both the reducibility and redox behavior of the catalysts play a key role on the CO oxidation reaction.
Figure 3C and D show soot conversions to CO_x as functions of temperature over nanostructured and SCS-based catalysts under "tight" catalyst-soot contact. To sum up, nanostructured ceria-based catalysts perform better than the SCS-based counterpart, despite the lower BET surface areas. Structural properties of ceria-based catalysts strongly influence soot oxidation activity. For the nanostructured materials, the increasing order of soot oxidation activity is:

$$Ce_{0.9}Zr_{0.1}O_2\text{-}NP < CeO_2\text{-}NP < Ce_{0.9}Pr_{0.1}O_2\text{-}NP < Ce_{0.8}Zr_{0.1}Pr_{0.1}O_2\text{-}NP$$

This finding confirms that praseodymium contributes positively towards the soot oxidation reaction over nanostructured catalysts. On the other hand, the SCS-based catalysts exhibit similar catalytic performance, except for the $Ce_{0.9}Zr_{0.1}O_2$-SCS sample, which is the least performing catalyst. Then, dopants like Zr and Pr species does not promote the soot oxidation activity. Moreover, the incorporation of Zr into the ceria lattice does not have a direct beneficial effect on the soot oxidation for catalysts calcined at mild temperature, since it decreases the surface redox centers, which are directly dependent on the Ce^{3+}-Ce^{4+} surface density.

Acknowledgments
The Ministero dell'Università e della Ricerca (MIUR) (grant number: RBFR12LS6M 001) is acknowledged for sponsoring this research activity (FIRB - Futuro in Ricerca 2012).

REFERENCES

1. Trovarelli A. Fornasiero P., *Catalysis by ceria and related materials*, London: Imperial College Press, 2013.
2. Duprez D., Cavani F., *Handbook of advanced methods and processes in oxidation catalysis*, London: Imperial College Press, 2014.
3. Wu Z., Li M. Overbury S.H., *J. Catal* 285: 61-73 (2012).
4. Freund H.J., Meijer G., Scheffler M., Schlogl R. Wolf M., *Anghew Chem Int Ed* 50: 10064-10094 (2011).
5. Royer S. Duprez D., *ChemCatChem* 3: 24-65 (2011).
6. Piumetti M, Bensaid S., Russo N., Fino, *Appl. Catal. B* 165: 742-751(2015).
7. Piumetti M., Bensaid S., Russo N. Fino D., *Appl. Catal B* 180: 271-282 (2016).
8. Piumetti M., Bensaid S., Fino D., Russo N., *Appl. Catal B* (2016).
DOI: 10.1016/j.apcatb.2016.02.023
9. Piumetti M., Bensaid S., Fino D., Russo N., *Appl. Catal B* 165: 742-751 (2015).
10. Andana T., Piumetti M., Bensaid S., Fino D., Russo N., Pirone R., *Appl. Catal B*
DOI: 10.1016/j.apcatb.2015.12.030 (2015).

doi: 10.4405/39proci2016.IV2